nature geoscience

SUPPLEMENTARY INFORMATION

DOI: 10.1038/NGEO2082

Modern and glacial topical snowlines controlled by sea surface temperature and atmospheric mixing

Aradhna K. Tripati*, Sandeep Sahany, Dustin Pittman, Robert A. Eagle, J. David Neelin, Jonathan L. Mitchell, Luc Beaufort

*Corresponding author: E-mail: aradhna.tripati@gmail.com, Phone: +1-626-376-1308

This PDF file containing supplementary information includes:

1. **Supplementary Methods**
2. **Figures S1-3**
3. **References**

Supplementary Tables, code, and data used for this study are also available for download as separate files.

1. Supplementary Methods

A. Samples from the warm pool

We measured planktic foraminifera and bulk sediment (primarily coccoliths) from three cores in the warm pool: MD97-2138 (1.420°N, 146.236°E, 1900 m water depth), Ocean Drilling Program Site 806 (0.319°N, 159.361°E, 2519.9 m), and V24-109 (0.433°N, 158.8°E, 2367 m). Monospecific samples of *Globigerinoides ruber* (white) and *G. sacculifer* (without sac) from the >250 μm size fraction were analyzed. Published age models for these sites were used, and are based on radiocarbon (MD97-2138)[1] or correlation of calcite $\delta^{18}O$ data with published isotopic records (ODP Site 806 and V24-109)[2,3]. Individual results are in Table S1 and sample averages are reported in Table S2. Means for different time intervals are reported in Table S3.

B. Modern temperature and relative humidity data for the warm pool

Fig. 1 in the main text shows average summer (June-July-August) air temperatures at the 600 millibar pressure level (for 1979-2010; NCEP2 re-analysis dataset) as well as the Reynolds re-analysis SSTs[18] from 1982-2010. Climatological average SSTs for the warm pool are 29.4°C as shown in Fig. 2B and vary by less than 0.4°C seasonally. Surface water $\delta^{18}O$ values are from a published database[4]. The average surface water $\delta^{18}O$ value for the region is 0.4‰ (V-SMOW) and is shown in Fig. 2C.

Fig. 3A and 3C show observed mean vertical temperature profiles from the DOE Atmospheric Radiation Measurement (ARM) program's observations at Nauru, Manus, and Darwin[5,6]. These three sites were chosen because of their location in the warm pool and their varying degrees of continentality. Individual soundings have uncertainties of ~0.5°C and the long-term average profile for each site has an error that is <0.5°C. Data for Nauru and Manus were processed as part of D. Pittman's M.Sc. thesis[7]. For the profiles in Fig. 3A and 3C, the width of the observed lines gives the spread between the mean of all soundings and conditions typical of deep convection (above ~500 m which is approximately the mean height of the convective cloud layer). Specifically we calculated two mean temperature profiles for each site: one using all data, and a second using observed means during convective conditions (i.e., "conditional" means corresponding specifically to periods when column water vapour exceeded a threshold of 60 or 65 mm which biases the mean profile towards periods of deep convection). The profiles from all of the sites are similar with the exception of some of the results from Darwin (which shows seasonal convective variability and therefore has a mean profile which is slightly different from the other five profiles). Relative humidity data from these sites was also used in this study. The ARM datasets from Nauru, Manus, and Darwin used in this study are provided as supplementary files in .dat format.

C. Introduction to clumped isotope thermometry

Clumped isotope thermometry is based on the principle that ordering, or 'clumping', of heavy isotopes into bonds with each other in molecules is a temperature-dependent phenomenon. In carbonates, rare heavy isotopes (^{13}C, ^{18}O) occur in a pool of light abundant isotopes. Carbonate 'clumped isotope' thermometry examines the proportion of ^{13}C and ^{18}O that are bound to each other within the carbonate mineral lattice[8]. The extent of ordering is predicted to be temperature dependent based on theoretical calculations, with disorder increasing as temperature increases[9].

The basis for the clumping of these heavy isotopes into bonds with each other is thought to be the thermodynamically controlled exchange of stable isotopes amongst isotopologues of carbonate ion[10,11]. The equilibrium constant for the reaction:

$$^{12}C^{18}O^{16}O_2^{2-} + {}^{13}C^{16}O_3^{2-} = {}^{13}C^{18}O^{16}O_2^{2-} + {}^{12}C^{16}O_3^{2-}$$

forms the theoretical basis for carbonate clumped isotope thermometry, with the doubly substituted species (or heavy isotope "clump") slightly more stable than the other isotopologues, and a progressively more random distribution of heavy isotopes amongst all possible isotopologues preferentially favored with increasing temperatures. So in an equilibrium precipitate, if the equilibrium constant for the above reaction is known and the abundance of all four isotopic species is measured, the temperature can be calculated independent of the isotopic composition of the water in which the carbonate grew. In addition, clumped isotope-derived temperatures can be combined with carbonate $\delta^{18}O$ to estimate water $\delta^{18}O$, by applying an appropriate carbonate-water oxygen-isotope fractionation relationship[12,13].

In practice, carbonate 'clumped isotope' thermometry is based on analyses of $^{13}C^{18}O^{16}O$ in CO_2 produced by acid digestion of $CaCO_3$. The abundance of this species is reported using the notation Δ_{47}, representing the mass 47 enrichment in CO_2 relative to the amount of mass 47 expected for a CO_2 that has the same bulk isotopic composition but a stochastic distribution of isotopologues, in units of ‰. Specifically Δ_{47} is defined as[14]:

$$\Delta_{47} = \left[\frac{R^{47}}{2R^{13} \cdot R^{18} + 2R^{17} \cdot R^{18} + R^{13} \cdot \left(R^{17}\right)^2} - \frac{R^{46}}{2R^{18} + 2R^{13} \cdot R^{17} + \left(R^{17}\right)^2} - \frac{R^{45}}{R^{13} + 2R^{17}} + 1 \right] \cdot 1000$$

where R refers to the ratio of the minor isotopologue to the major isotopologue of the molecule (or atom) of interest.

D. Clumped isotope systematics in foraminifera and coccoliths

The work we have done previously includes a detailed survey of the 'clumped isotope' composition of multiple modern marine species that are widely used in paleoceanography[10]. The results of our study showed that the proportions of ^{13}C-^{18}O bonds in benthic and planktic foraminifera and coccoliths are not subject to resolvable disequilibrium biological fractionations, and are independent of the composition of the water in which the mineral precipitated. We calibrated the thermometer with 41 samples of foraminifera and coccoliths that are independently known to have grown at temperatures ranging from -0.9 to 29.2°C, including both calcitic and aragonitic taxa. Two cultured samples of coccoliths and three cultured samples of benthic foraminifera have also been measured. We have also investigated the results of different cleaning techniques. In total, 20 species have been surveyed, and ~150 analyses were made for the calibration study[11].

As part of our calibration work, we showed the Δ_{47} values of modern foraminiferal and coccolithophorid samples (and bulk carbonate comprised predominantly of coccoliths) exhibit a negative correlation with calcification temperature[10]. All data for measured cultured and core-top samples fall within error of an independently measured inorganic calcite calibration line[8] and a recently published calibration for biogenic carbonates[15]. The lack of detectable taxon-specific effects, or salinity and carbonate ion effects in foraminifera and other biogenic carbonate Δ_{47} calibration datasets[10,15], over the range likely to be of important from the LGM-recent, contrasts with what is known from foraminiferal Mg thermometry[16–20].

Given the taxonomic breadth represented by these samples, this result suggests that foraminifera and coccoliths grow at equilibrium with respect to their proportions of ^{13}C-^{18}O bonds. A second study of foraminifera has recently been published by another group[21] and reproduced our results. Fig. S1 shows that paired measurements of Δ_{47} in foraminifera and bulk carbonate in the same sample for this region are comparable.

E. Clumped isotope analyses

Samples were cleaned to remove secondary carbonates and organic matter using a published method[10]. In total, we made 51 analyses (including replicates) of samples for this project. Each sample was composed of several hundred to a few thousand foraminifera or tens of thousands or more coccoliths. Sample digestion and analysis occurred on specially modified Thermo Fisher 253 gas source mass spectrometers dedicated to measuring clumped isotopes in CO_2 at UCLA and Caltech. Samples and standards are processed using a custom-built automated system for digestion and purification[22] is attached to a gas-source mass spectrometer that has been configured for the analysis of multiply substituted isotopologues of CO_2. The carbonate sample digestion system is composed of 1) a Costech Zero Blank autosampler made of stainless steel that will pull high vacuum, 2) a common acid bath for phosphoric acid digestion of samples, 3) cryogenic traps (dry ice and ethanol, and liquid nitrogen) for the purification and collection of CO_2 and removal of water and other gases with low vapor pressures, 4) a gas chromatograph with a packed column and a cryogenic trap to further purify CO_2 through the removal of organic contaminants, with helium being used as a carrier gas, 5) cryogenic traps to separate prepared gases from the helium, 6) a final set of valves and traps to purify CO_2 and transfer it into the bellows of the mass spectrometer.

In this system, between 4-12 mg of sample is digested at 90°C in phosphoric acid (density = 1.92 g/ml) in order to ensure a sufficient amount of CO_2 for stable voltages over the course of several hours. The reaction time was 20 minutes in a common acid bath system, with acid changed after every 10-15 analyses. The resultant gas was actively pulled into a metal trap immersed in liquid N_2, passing through a glass water trap immersed in a dewar of ethanol at -70ºC. After two rounds of cryogenic purification to remove water, CO_2 was then passed through a gas chromatograph containing a column filled with PoraPak Q that is at -20ºC, and then recleaned cryogenically as described above to remove any additional water before being transferred to the inlet of the mass spectrometer. The sample gas was analysed for masses 44 to 49 AMU on a Thermo 253 gas source isotope ratio mass spectrometer. Measurements are made to yield a stable 16-volt signal for mass 44, with peak centering, background, and pressure balancing before each acquisition, and each acquisition is comprised of eight sample-working gas measurement cycles. These conditions were selected to ensure stable ion currents and minimize time-dependent fractionation of sample and reference gas reservoirs. The total analysis time (including peak centering, background measurement, and pressure balancing) ranged from between 4 and 8 hours.

At UCLA, we analyzed 'heated gases' with different bulk isotope compositions and 25°C water-equilibrated gases. Heated gases are composed of CO_2 with a stochastic distribution of isotopes between isotopologues. They are prepared using from gas standards with different bulk $\delta^{18}O$ and $\delta^{13}C$ ratios. These gases are cryogenically cleaned and then sealed in quartz breakseals that are subsequently heated to 1000°C for two hours and quenched at room temperature. At UCLA, approximately three standard analyses (both gas standards and carbonate standards) and two to four sample analyses were performed each day. At Caltech, each day we analyzed a heated gas composed of CO_2 with a stochastic distribution of isotopes between isotopologues. All standard gases are then purified and analyzed using the same protocol as sample gases[23].

Data are reported on both the internal reference frame (Table S1) and the absolute reference frame (Table S1). For data measured at Caltech, absolute reference frame calculations were done using a secondary transfer function based on mean standard values. The standard error of Δ_{47} values reported factor in uncertainties associated with these corrections.

We used published acid digestion fractionation factors for determining carbonate $\delta^{18}O$ ratios. The value used for calculating calcite $^{18}O/^{16}O$ ratios from analyzed CO_2 is 1.00821 for samples digested at 90°C[24]. For calculations of equilibrium $^{18}O/^{16}O$ ratios in calcite (and to calculate $\delta^{18}O$-calcification temperatures), we used a published relationship[8] to describe calcite-water fractionation: $1000 \ln \alpha_{calcite-H_2O} = \frac{18.03 \times 10^3}{T} - 32.42$, where T is temperature in Kelvin.

The presence of organics can yield significant isobaric interferences with CO_2 isotopologues that can impact both accuracy and precision, resulting in an apparent temperature bias and/or larger internal errors. We monitored masses 48 and 49 to screen for isobaric interferences from the presence of these compounds. No data were deemed to be from a contaminated sample.

F. Precision

We report mean sample Δ_{47} values and the standard error of each sample mean in Table S2. Error propagation factored in uncertainty in measurement of the Δ_{47} of CO_2 and uncertainty in reference frame calculations. Several of the measurements of foraminifera and coccoliths made in this study required a substantial increase in counting times and numbers of replicated samples, relative to past clumped isotope studies, in order to achieve precisions appropriate for paleoceanographic application. Most of these data are relatively precise (s.e. of 0.005-0.011‰) and have approximately half the uncertainty typical of such data (0.011-0.025‰)[23]. In some cases, the standard error for each sample mean was reduced to ~0.003‰ or better, corresponding to temperature uncertainties of ±0.5-0.8°C (1 s.e.). Low errors similar to are achievable through the measurement of large samples, many replicate analyses, and sample pre-treatment to remove organic contaminants that can introduce isobars within the relevant mass range.

G. Accuracy

We measured multiple standards repeatedly, typically every 4-10 analyses, in order to determine accuracy and monitor long-term external precision. Stable isotope ratios for standards are statistically indistinguishable at the 95% confidence level to those previously reported[8,10,10,22,23]. These standards included NBS-19. Replicate analyses in both labs yielded a mean Δ_{47} of 0.350‰ ± 0.008‰ (1 s.e.) on the internal reference frame and 0.392 ± 0.009‰ (1 s.e.) on the absolute reference frame (compared to accepted values of 0.352 and 0.392‰). The average measured $\delta^{18}O$ (V-PDB) for this standard was -2.193‰ ± 0.031‰, and $\delta^{13}C$ (V-PDB) was 1.845‰ ± 0.099‰.

H. Calculations of temperature and water $\delta^{18}O$

Δ_{47} values are converted to temperature in three ways. As shown in Tables S1-S3, the choice of calibration does not affect our conclusions. First we used the published inorganic calibration[8] which we have shown in a previous calibration study[10] to be appropriate for these

species of planktic foraminifera, cultured coccoliths, and bulk sediment with a carbonate fraction that is composed primarily of coccoliths. This calibration was (1) applied to Δ_{47} values on the internal reference frame, and (2) on the absolute reference frame. (3) We also calculated temperatures by applying a published biogenic calibration to data on the absolute reference frame. This calibration is based on a much more extensive amount of data[15] and also fits the data for these types of carbonates extremely well. Therefore figures in the main text and values used refer to calculations done using the biogenics calibration (using Δ_{47} values on the absolute reference frame), although our conclusions are not impacted by choice of calibration (see Table S3 for comparison of absolute temperatures and temperature differences calculated using all three calibrations).

Our analyses of downcore bulk sediment yields statistically indistinguishable results from those of shallow-dwelling planktic foraminifera, consistent with our observations that cultured coccoliths and core-top bulk sediments record equilibrium Δ_{47} values[10]. The presence of benthic foraminifera in bulk sediment is estimated to potentially bias our downcore measurements by a negligible amount due to their low abundance (up to 0.06-0.09°C).

Water isotope ratios are reported relative to V-SMOW. Surface water $\delta^{18}O$ ($\delta^{18}O_{sw}$) is calculated by applying an appropriate $\delta^{18}O$-temperature calibration[12,13] to Δ_{47}–derived temperatures from either bulk carbonate or planktic foraminifera in combination with planktic foraminiferal $\delta^{18}O$ values. Water isotope values for planktic foraminifera are calculated using a published equation from Bemis et al.[13] for *Orbulina universa* cultured at low-light levels, whereas for bulk carbonate samples, the inorganic calcite equation of Kim and O'Neil[12] was used. These equations were chosen because application to core-top and late Holocene samples yielded accurate water isotope values for the region[25].

Ice volume-corrected values of seawater $\delta^{18}O$ for the region are shown in Fig. 2C and are calculated by subtracting a record of global ocean $\delta^{18}O$ from surface water $\delta^{18}O$. Global ocean $\delta^{18}O$ is controlled by fluctuations in continental ice storage, and is estimated using published sea level estimates[26] and a $\Delta\delta^{18}O$-Δsea level relationship of ~0.08‰/meter sea level. For comparison, we also used an unpublished compilation of sea level data (Adkins, pers. comm.) and found that application of the two different sea level histories produced global ocean $\delta^{18}O$ values that agree to within 0.04‰ except at 28 ka, where they differ by 0.15‰.

I. Clumped isotope errors in comparison to other marine paleotemperature proxies

Although the errors in individual sample measurement for this proxy (>°1 C) are larger than what is typically reported for Mg/Ca thermometry, by measuring many replicate samples (e.g., n = 20 for the LGM), we are able to reduce this source of uncertainty to <°1 C (Fig. S2). Another source of uncertainty stems from how representative measurements of samples are of the mean for a region and for the time interval being studied. Due to the large sample masses required and large numbers of individual tests (or coccoliths) per sample, our results should reflect a long-term regional mean for the LGM, despite the limited temporal resolution of our records.

Another source of uncertainty inherently stems from the extent that assumptions are required to apply a proxy. Given the lack of 'vital' effects in planktic foraminifera and bulk sediments, the contribution of this uncertainty is minimal compared to other proxies (i.e., Mg/Ca thermometry, alkenones, transfer functions).

We note that the Holocene structure of our record is similar to alkenone SST records reconstruction for this time interval, and less similar to some Mg/Ca reconstructions which

are interpreted to reflect constant SST during the Holocene[1,2]. The LGM-recent record shows a structure which is generally coherent with alkenone and oxygen isotope records[1].

However, the magnitude of the LGM-late Holocene and LGM-WOA shift is most consistent with the salinity-corrected Mg/Ca, and then the regular Mg/Ca-based reconstructions, and less similar to alkenone-derived reconstructions[1,27,28]. Some of these differences may reflect the different sample size requirements for each of these techniques, which may influence how much time is being represented by a single sample.

J. Calculation of LGM-Recent temperature changes shown in Fig. 2

In the main text, Figure 2 shows a comparison of LGM-recent temperature change estimated using clumped isotope data to other published estimates for the WPWP and other tropical regions. Estimates of mean temperature change in the WPWP are based on pooling together data from multiple sites and samples to develop a statically robust estimate for the region (Table S3). Proxy-based estimates are calculated to be consistent with the MARGO compilation[27] (where the published data for Mg/Ca, alkenones, and transfer functions are derived), who reported results as average LGM SSTs for region minus annual mean from climatology. Error bars representing 1 s.e. (Δ_{47}, Mg/Ca, alkenone, transfer function) and range of estimates (coral Sr/Ca). LGM temperatures are also calculated from 23-19 ka to be consistent with the MARGO synthesis. Results from PMIP2[29] and PMIP3/CMIP5[30] climate model simulations. Values from climate model simulations represent the difference in annual mean SSTs between LGM and pre-industrial simulations for 15°N-15°S and 140-165°E, with vertical bars showing the range of SSTs in the region. Mg/Ca, alkenone, and transfer function SSTs are from a published compilation[27], Sr/Ca results are from a publication[31].

The clumped isotope-based reconstruction of average WPWP temperatures and water $\delta^{18}O$ for the over the last 30,000 years in Panel B is based on measurements of mono-specific samples of planktic foraminifera (*Globigerinoides ruber* (white) and *G. sacculifer* (without sac)) or bulk sediment (primarily coccoliths) from 3 sites in the WPWP. Climatological average temperatures for the warm pool are 29.4 ± 0.4°C. LGM temperatures are 25.3 ± 0.2°C (1 s.e.; 5 samples and 20 analyses in total; 1σ is 0.4°C). LGM – climatological differences are calculated as -4.1°C ± 0.2°C (2 s.e.) and LGM-core-top differences are -4.7 ± 0.8°C (2 s.e.). These values are also reported in Table S3.

Note the temporal variation observed in the clumped isotope-temperature and water $\delta^{18}O$ estimates is similar to the structure of Mg/Ca-based reconstructions[1]. In Panel C, LGM water $\delta^{18}O$ values are -0.2 ± 0.1‰ (ice volume-corrected or local seawater $\delta^{18}O$ ratios). Unadjusted values are 0.8‰. The modern average is 0.4 ± 0.1‰[25] compared to reconstructed core-top values of 0.5 ± 0.1‰. These values are also reported in Table S3.

K. Tropospheric temperatures modelled as an adiabat

As a parcel of air warms up at the surface, it becomes less dense than the environmental air surrounding it resulting in an upward vertical force against the parcel. Freezing level calculations were done for an air parcel following an adiabat, using present-day conditions over the warm pool: near-surface air temperature of 28.8°C and near-surface relative humidity of ~81%. The present-day freezing level assuming an adiabatic ascent is ~6 km which is ~1 km above the observed value (Fig. 3A; Table S4). Since an adiabatic model does not take into account entrainment of environmental air by the parcel, it has a relatively lower lapse rate and hence a higher freezing level. Therefore a moist adiabat is clearly not a

good approximation of observed mean tropical tropospheric temperature profiles, including for sites with differing degrees of continentality.

L. Simulating the absolute elevation of glacial snowlines using an adiabat

It can be seen from Fig. 3A that an adiabat significantly overestimates the modern freezing level, and from Fig. 3B and S3 that it also significantly overestimates the LGM freezing level (by close to 800 m). We estimated the changes in near-surface relative humidity required for an adiabat to match the snowlines of the modern and LGM: the reduction in surface relative humidity for the modern to match snowline data (and radiosonde data) is ~19%. For the LGM, reductions of ~27%, ~22%, ~16%, and ~10%, are required to reconcile surface temperature (T_S) changes of 2°C, 3°C, 4°C, and 5°C, respectively, with snowline data. Thus, if one were to model the tropical tropospheric temperature using a moist adiabat, unrealistic deviations from estimated surface relative humidity need to be invoked, both for the modern and LGM, in order to match snowline data and other constraints on freezing levels.

M. Description of convective entrainment

The role of convective entrainment was considered in this study because the consideration of an upward moving air parcel as a closed system is not accurate. Air parcel properties will mix with the surrounding environmental properties (typically lower temperature and drier air). This entrainment of drier air causes the air parcel to be undersaturated with respect to its environment thus increasing its lapse rate away from the hypothetical moist adiabat and subsequently cooling the parcel at a faster rate. In addition to cooling the air parcel at a faster rate, entrainment also creates an unstable environment for the rising parcel consequently enhancing deep convection.

N. Radiative-convective calculations of tropospheric temperatures considering entrainment

To calculate tropospheric temperature profiles, we created a procedure that is as close as feasible to the simplicity of a moist adiabat but which takes into account the impact of entrainment of environmental air in the troposphere. While the moist adiabat requires specification only of near-surface air temperature and specific humidity, the entraining plume calculations require environmental air temperature and relative humidity as a function of height. The temperature is computed using a radiative-convective equilibrium model. For the present day, the relative humidity is taken from observations at Nauru[5,6].

For the LGM, the present-day values relative humidity values were also used as a standard case, and the impact of specified changes in relative humidity relative to present day is evaluated. We test several different specifications of the change in relative humidity: specification of the vertical profile of relative humidity change evaluated from climate model simulations of LGM and of preindustrial climate; specification of relative humidity change profiles taken from current day observations but with conditional averages on low or high precipitation; and an idealized profile in which the relative humidity change is vertically constant in the free troposphere, with a blending zone (below 800 mb) to a specified change in surface relative humidity (set to zero for simplicity for the standard case presented in the text, and then evaluated separately).

For the calculations involving entrainment, the large-scale temperature profile must be computed as well as the temperature profile within the convecting plume. These computations are done using a radiative-convective equilibrium model. It is thus necessary to

specify both a convective scheme and a radiative cooling term. However, because the convection time scale is relatively short compared to that of radiative cooling, the computation is not very sensitive to the details of either of these, as the entrained large-scale temperature is only slightly cooler than that of the parcel. Specifically, the environmental temperature above the boundary layer is calculated as a modified radiative-convective equilibrium using a modified Betts-Miller convective scheme[32] that adjusts the large-scale temperature towards that of the entraining convective plume. To consider the effects of entrainment on vertical temperature profiles, we needed a model that computes its temperature interactively as we go up from the surface, including temperature inside and outside the plume. A Betts-Miller scheme was chosen because is one of the simplest convective models that we can do this computation with, and has the advantage that the assumptions are very transparent.

O. Code used for entraining plume calculations

The IDL code used in this study for the radiative-convective equilibrium model calculations is adapted from previous publications[33,34]. It is included as a supplementary file labelled "main.pro" along with other files that contain additional functions for thermodynamic computations and datasets analyzed (see Section 1H of this file) as part of this study.

P. Details of entraining plume calculations

The cooling term (which can include a large-scale dynamical component) is approximated as independent of height in the lower free troposphere. Standard case cooling of 1.5ºC/day and Betts-Miller 0.1 day convective time scale yield a single combined parameter of a 0.15ºC difference between environment and convective plume temperature. The applicability of small temperature difference can be motivated observationally by looking at the large-scale temperature as seen in soundings under all conditions versus under conditions of strong convection. The observed small range between average temperatures and those occurring under strong convection (as estimated by the column water vapor succeeding 65 mm) is seen as a narrow range in Fig. 3A and 3C. The consequence of the small temperature difference between the large-scale on the convective parcel in the entraining calculations is that the departures from the moist adiabat depend almost entirely on the entrainment of subsaturated environmental air in the free troposphere.

The computation transitions in the boundary layer to specification of near-surface air temperature over the lowest 10 mbar. This avoids dependence on computation of surface or top of atmosphere energy balance and permits straightforward examination of the factors affecting lapse rate between surface and the freezing level. Near-surface air temperatures are assumed to closely track the sea surface temperature as they do in the modern tropics (~0.5-1.0°C cooler than SSTs) as seen in the COADS dataset and reported previously[35].

To obtain relative humidity profiles under conditions where convection is active in the lower free troposphere, we use soundings for which there is at least a minimum level of precipitation (0.005 mm/h average from one-minute resolution optical gauge data) over a three-hour window about the sounding time. This defines our standard case profile (which has a mass-weighted vertical average relative humidity through the lower free troposphere (1-5 km) of 76%. Sensitivity is then evaluated over a broader set of conditions, discussed below. The mixing process conserves the ice-liquid water potential temperature[36] which reduces to the reversible liquid water potential temperature for the range of interest here. The entrainment coefficient, specifying the fraction of environmental air mixed with the parcel

per unit ascent in pressure coordinates, is taken constant in vertical and is calibrated so the environmental temperatures yield a close match to the observations near the freezing level. Fig. 3 of the main text shows that the profile matches well over the entire lower troposphere.

Q. Uncertainties in relative humidity

In Tables S6-S8, we estimate sensitivity of calculated freezing levels to uncertainties in a range of parameters (near-surface temperature, surface relative humidity, entrainment coefficient, and free tropospheric relative humidity). The latter represents the largest true uncertainty when considering LGM paleoclimate.

We estimate sensitivity of the freezing level change calculation to uncertainties in the parameters fit to recent observations as follows, in order to quantify model parameter degeneracy. Any set of parameters is required to fit the modern observed temperature profile. The impact of combinations matching this criterion on the change in freezing level when near-surface air temperature is reduced by a specified amount (4ºC in the standard case) is then evaluated. Alternatively doubling the radiative cooling and setting it to vanishingly small values, with the entrainment parameter respectively decreased/increased by 10% to match modern soundings, the range on the change in freezing level is roughly ±15 m about the standard case of 930 m (freezing level changes are rounded to nearest 5 m). Thus a small ensemble of variations in precipitation threshold for choosing relative humidity soundings in the above procedure yielded a range of only ±15 m.

To generate highly conservative error bars based on convective thresholds, the following procedure was used to determine an outer bounds on the range of relative humidity. An average over a nonprecipitating (less than 0.0025 mm/h in a three-hour window) set of soundings, and an average over a set associated with very strong deep convection (precipitation rate greater than 2.56 mm/h averaged over a three-hour window) were chosen to obtain relative humidity profiles spanning dramatic changes in convective regime. The mass-weighted average relative humidity through the lower free troposphere (1-5 km) for these cases was 63% and 84%, compared to the standard case average of 76%. For the nonprecipitating relative humidity profile case, and entrainment coefficient of 0.0018 hPa^{-1}, i.e. approximately half the standard case value of 0.0035 hPa^{-1}, was used to recalibrate to observed temperature profiles. For the strongly precipitating profile case, the entrainment coefficient was almost doubled to 0.0062 hPa^{-1}. When the LGM 4ºC surface temperature shift was undertaken in each case, the resulting freezing level changes were 955 and 910 m respectively, i.e. approximately +25 m and -20 m differences relative to the standard case. Further tests replacing observed relative humidity profiles with vertically constant approximations yielded similar results, as expected since the entrainment process integrates over the layer. Overall, the constraint of matching modern observed temperature profiles keeps sensitivity of freezing level change to the calibration process to less than half of the error bars on the glacial elevation change, before taking into account the larger uncertainty associated with possible changes in relative humidity.

We now address the question of error bars associated with possible changes of relative humidity in LGM warm-pool climate relative to present day. It is important to recall that because wave processes reduce pressure gradients in the horizontal near the equator the temperature profile is set by convection over a large horizontally-influenced region. This is the reason for the strong similarity of the vertical temperature profiles at the sites studied. The statistics of relative humidity in the free troposphere that would have to change in LGM in order to impact the lapse rate would have to apply over a substantial spatial region in the warm pool, not just locally at an observation site.

The first means of assessing possible relative humidity changes is to examine climate model simulations. Differences in the profiles of free-tropospheric relative humidity were evaluated over a warm pool box average (12.5°S-9.5°N, 137.5°E-176.9°E) between LGM and pre-industrial simulations of the available CMIP5 models. This ensemble included CCSM4, CNRM, MIROC, MPI, IPSL and GISS. The relative humidity differences exhibited a range in free-tropospheric vertical average of -2.1% to 0.5% (ensemble mean of -0.6%), consistent with the hypothesis of small changes in relative humidity. To match the midpoint of the range in observed change in freezing level, with all parameters at the standard values but using the vertical profiles of the change in RH from these endpoint models (IPSL and MPI, respectively), the implied surface air temperature change ranges from -4.01 to -4.09°C. In other words, the range of uncertainty in surface temperature change implied by this model estimated range of free tropospheric relative humidity is small. The surface temperature change in these models is smaller than that estimated here (3.3 and 2.0° C cooling, respectively, for the endpoint models above). However, if one considers doubling the size of the error bar to conservatively account for this, it still yields only a small error bar, less than ±0.1°C, associated with these relative humidity changes.

A second means of assessing possible error bars associated with changes in free tropospheric relative humidity, if one does not trust the model results, is to consider the extreme range that might occur if precipitation was almost entirely shut down or were to increase to intensities typical of the most intensely precipitating three hourly intervals. This will almost certainly yield an overestimate with respect to what is achievable in climate changes and can be regarded as an extreme outer bound on the free tropospheric relative humidity changes that can occur even with a strong change in convective regime. These values yield a range of free tropospheric relative humidity differences between averages of +3% for times of heavy precipitation to -9% for times of no precipitation, respectively. To match the midpoint of the range in observed change in freezing level, with other parameters at the standard values, these would imply surface air temperature changes of -4.6° C to -2.5° C. In other words, to account for a change as small as -2.5° C in surface air temperature through changes in free tropospheric relative humidity alone would require a large region of the warm pool to undergo a reduction in precipitation corresponding to that found in Nauru present day observations for very dry three-hourly precipitation bins (values between 0.002 and 0.02 mm/hr).

A third way of assessing possible error bars associated with changes in free tropospheric relativity is to ask what changes that would be required for the endpoints of the surface thermometry error range to fall within the range of uncertainty in the change in freezing level from glacial elevation data. The 12% relative humidity reduction required for a 3ºC surface temperature decrease to match 900 m freezing level change exceeds the bounds of the most conservatively estimated range from the previous two calculations. Similarly, the 10% relative humidity increase required for a 5ºC decrease to match 1000 m freezing level change is so large compared to either the range from the models or the conservative range for extremely wet cases that these appear dynamically highly improbable.

Changes in surface relative humidity are strongly constrained by boundary layer balances and moisture supply from the ocean[8] but a 2% decrease can yield roughly 80 m in freezing level change in addition to those computed above.

The physical hypothesis is that properties of convective turbulence do not change between modern and LGM, and therefore that the entrainment coefficient constrained by modern data applies to the LGM. For completeness, Table S8 quantifies sensitivity to this assumption with the relative humidity profile fixed to the standard case, for a much larger range of changes in LGM entrainment coefficient than would be physically plausible. There

is an approximately linear relationship between the entrainment coefficient and the snowline of around 60 m for every 10 % change in the entrainment coefficient.

In short, these calculations favor a narrower uncertainty range than a change in SSTs of 3-5ºC and are more consistent with the 4-5ºC implied by the clumped isotope data. A match to the LGM snowline data assumes SSTs of 24.5-25.5°C, up to 2-4% reduced surface relative humidity, -5% to +1% changes in free tropospheric relative humidity, and entrainment similar to modern.

2. Supplementary Figures

Fig. S1

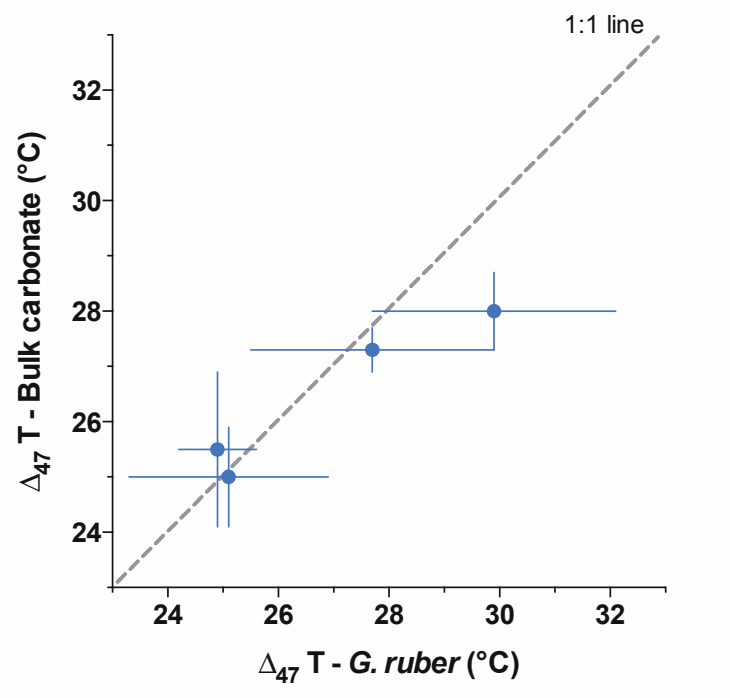

Fig. S1: Comparison of downcore Δ_{47}–temperatures from measurements of *G. ruber* and bulk carbonate from the same sample demonstrating both yield similar estimates of growth temperatures. Error bars represent 1 s.e., and values are from Table S2. 1:1 line is shown for comparison.

Fig. S2:

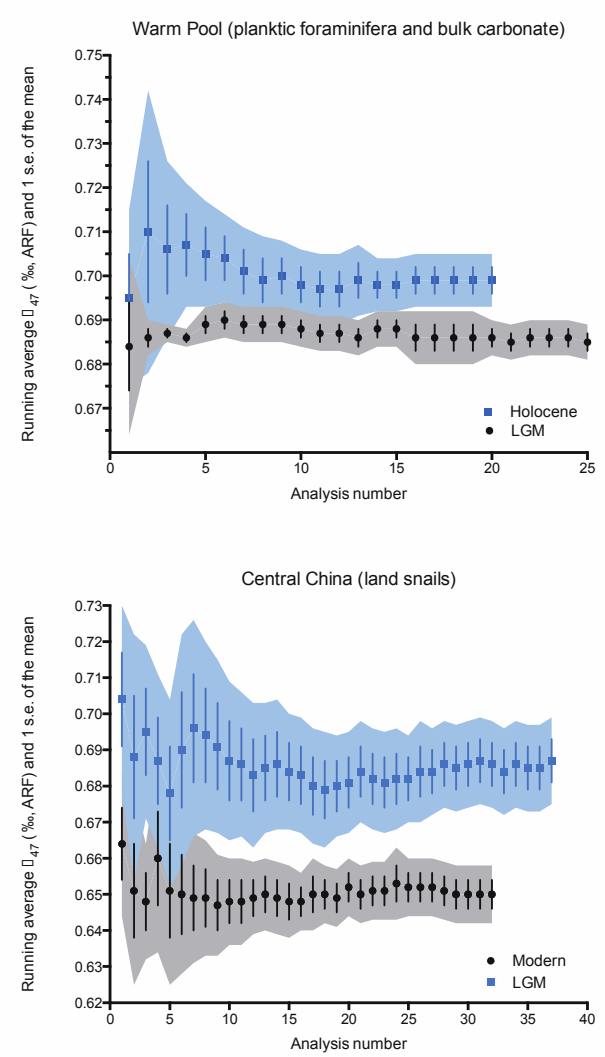

Fig. S2: Calculations of standard error for Δ_{47}–temperature proxy using data for replicate samples. Vertical error bars represent 1 s.e. and shaded regions represent 2 s.e. Each analysis was of a non-homogenized sample and therefore represented a true replicate (i.e., calcium carbonate sample was independently digested and purified before being analyzed on a mass spectrometer) that factored in sample heterogeneity, cleaning reproducibility, and analytical reproducibility. Actual data for LGM and Late Holocene samples for planktic foraminifera are from this study of the warm pool. Shown for comparison is an analysis of published data from individual terrestrial land snails from a site in China[37]. Note that marine samples of planktic foraminifera and of coccoliths would be expected to have much smaller errors than analyses of terrestrial snails due to the large numbers of individuals analyzed in each sample.

Fig. S3:

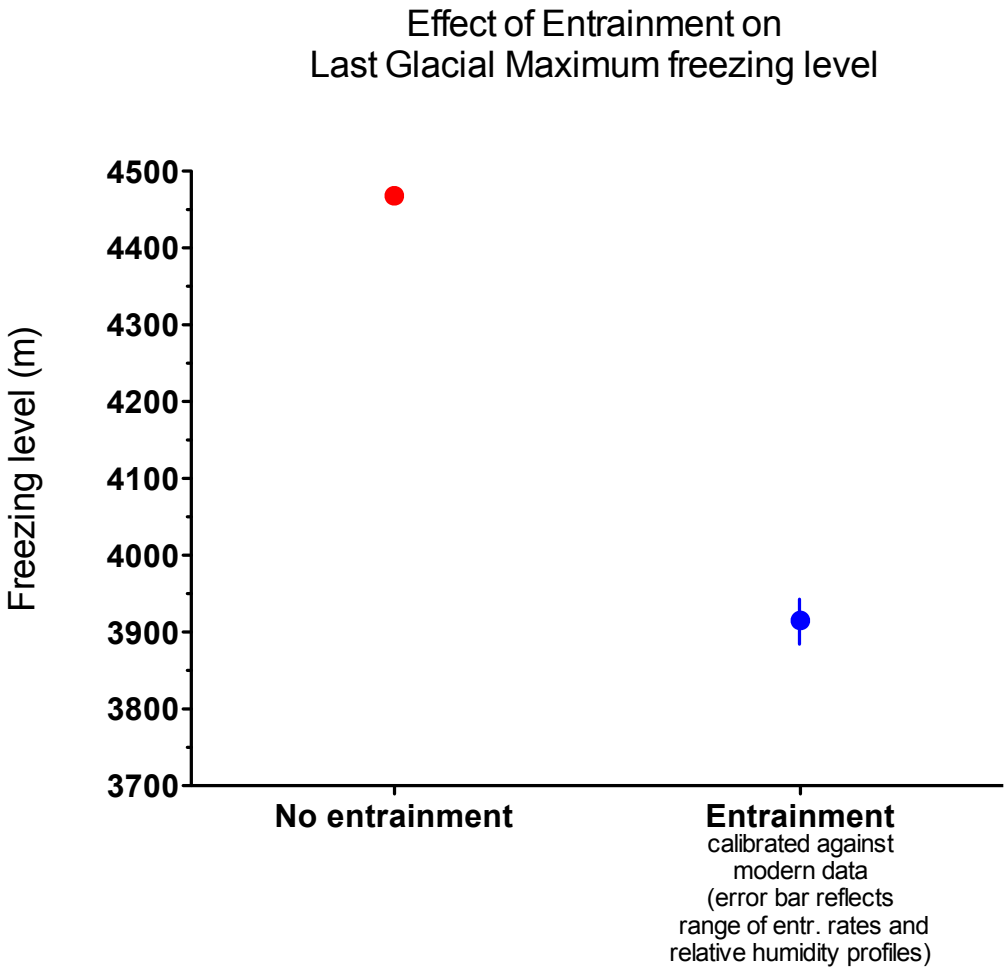

Fig. S3: Effect of including entrainment or just using an adiabat on snowline calculations for LGM. Calculations assume no change in relative humidity profiles and 5°C ΔSSTs (Table S8). Error bars reflect using a range of different entrainment coefficients constrained using modern data. The best match to the LGM snowline elevations and environmental lapse rates assumes ocean surface temperatures of 24.5-25.5°C, 2-4% reduced surface relative humidity, -5% to +1% changes in free tropospheric relative humidity, and entrainment similar to or slightly greater than modern.

3. References

1. De Garidel-Thoron, T. *et al.* A multiproxy assessment of the western equatorial Pacific hydrography during the last 30 kyr. *Paleoceanography* **22,** PA3204, doi: 10.1029/2006PA001269 (2007).
2. Medina-Elizalde, M. & Lea, D. The Mid-Pleistocene Transition in the Tropical Pacific. *Science* 310, 1009-1012 (2005).
3. Shackleton, N., Le, J., Mix, A. & Hall, M. Carbon isotope records from Pacific surface waters and atmospheric carbon dioxide. *Quaternary Science Reviews* **11**, 387-400 (1992).
4. Reynolds, R., Rayner, N., Smith, T., Stokes, D. & Wang, W. An improved in situ and satellite SST analysis for climate. *Journal of Climate* **15,** 1609–1625 (2002).
5. Stokes, G. & Schwartz, S. The Atmospheric Radiation Measurement (ARM) Program: Programmatic Background and Design of the Cloud and Radiation Test Bed. *Bulletin of the American Meteorological Society* **75,** 1201–1221 (1994).
5. Mather, J. *et al.* An Atmospheric Radiation and Cloud Station in the Tropical Western Pacific. *Bulletin of the American Meteorological Society* **79,** 627–642 (1998).
7. Pittman, D. Comparison of Community Climate System Model simulations and paleoclimate data for the Western Pacific Warm Pool climate during the Last Glacial Maximum. M.Sc. Thesis, UCLA (2012).
8. Ghosh, P. *et al.* ^{13}C-^{18}O bonds in carbonate minerals: A new kind of paleothermometer. *Geochimica et Cosmochimica Acta* **70,** 1439–1456 (2006).
9. Schauble, E., Ghosh, P. & Eiler, J. Preferential formation of ^{13}C–^{18}O bonds in carbonate minerals, estimated using first-principles lattice dynamics. *Geochimica et Cosmochimica Acta* **70,** 2510–2529 (2006).
10. Tripati, A. *et al.* ^{13}C–^{18}O isotope signatures and 'clumped isotope'thermometry in foraminifera and coccoliths. *Geochimica et Cosmochimica Acta* **74,** 5697–5717 (2010).
11. Eagle, R. *et al.* Body temperatures of modern and extinct vertebrates from ^{13}C-^{18}O bond abundances in bioapatite. *Proceedings of the National Academy of Sciences* **107,** 10377–10382 (2010).
12. Kim, S.-T. & O'Neil, J. Equilibrium and non-equilibrium oxygen isotope effects in synthetic carbonates. *Geochimica et Cosmochimica Acta* **61,** 3461–3475 (1997).
13. Bemis, B. *et al.* Reevaluation of the oxygen isotopic composition of planktonic foraminifera: Experimental results and revised paleotemperature equations. *Paleoceanography* **13,** 150–160 (1998).
14. Eiler, J. & Schauble, E. $^{18}O^{13}C^{16}O$ in Earth's atmosphere. *Geochimica et Cosmochemica Acta* **68,** 4767–4777 (2004).
15. Eagle, R. *et al.* The influence of temperature and seawater carbonate saturation state on ^{13}C-^{18}O bond ordering in bivalve mollusks. *Biogeosciences* **10,** 157–194 (2013).
16. Ferguson, J., Henderson, G., Kucera, M. & Rickaby, R. Systematic change of foraminiferal Mg/Ca ratios across a strong salinity gradient. *Earth and Planetary Science Letters* **265,** 153–166 (2008).
17. Mathien-Blard, E. & Bassinot, F. Salinity bias on the foraminifera Mg/Ca thermometry: Correction procedure and implications for past ocean hydrographic reconstructions. *Geochemistry, Geophysics, Geosystems* **10,** Q12011 (2009).
18. Lea, D., Mashiotta, T. & Spero, H. Controls on magnesium and strontium uptake in planktonic foraminifera as determined by live culturing. *Geochimica et Cosmochimica Acta* **63,** 2369–2379 (1999).
19. Kısakürek, B., Eisenhauer, A., Böhm, F., Garbe-Schönberg, D. & Erez, J. Controls on shell Mg/Ca and Sr/Ca in cultured planktonic foraminifera, *Globigerinoides rube*r (white). *Earth and Planetary Science Letters* **273,** 260–269 (2008).

20. Arbuszewski, J., Demenocal, P., Kaplan, A. & Farmer, E. On the fidelity of shell-derived ™$^{18}O_{seawater}$ estimates. *Earth and Planetary Science Letters* **300,** 185–196 (2010).
21. Grauel, A.-L. *et al.* Calibration and application of the 'clumped isotope'thermometer to foraminifera for high-resolution climate reconstructions. *Geochimica et Cosmochimica Acta* **108**, 125-140 (2013).
22. Passey, B., Levin, N., Cerling, T., Brown, F. & Eiler, J. High-temperature environments of human evolution in East Africa based on bond ordering in paleosol carbonates. *Proceedings of the National Academy of Sciences* **107,** 11245–11249 (2010).
23. Huntington, K. *et al.* Methods and limitations of 'clumped' CO_2 isotope (Δ_{47}) analysis by gas-source isotope-ratio mass spectrometry. *Journal of Mass Spectrometry* **44**, 1318-1329 (2009).
24. Swart, P., Burns, S. & Leder, J. Fractionation of the stable isotopes of oxygen and carbon in carbon dioxide during the reaction of calcite with phosphoric acid as a function of temperature and technique. *Chemical Geology* **86,** 89–96 (1991).
25. LeGrande, A. & Schmidt, G. Global gridded data set of the oxygen isotopic composition in seawater. *Geophysical Research Letters* **33,** L12604 doi:10.1029/2006GL026011 (2006).
26. Lambeck, K. & Chappell, J. Sea level change through the last glacial cycle. *Science* **292,** 676–686 (2001).
27. MARGO Project Members, Constraints on the magnitude and patterns of ocean cooling at the Last Glacial Maximum. *Nature Geoscience* **2,** 127–132 (2009).
28. Visser, K., Thunell, R., & Stott, L., Magniture and timing of temperature change in the Indo-Pacific warm pool during deglaciation. *Nature* **421,** 152–155 (2003).
29. Braconnot, P. *et al.* Results of PMIP2 coupled simulations of the mid-Holocene and Last Glacial Maximum- part 1: experiments and large-scale features. *Climate of the Past* **3,** 261–277 (2007).
30. Braconnot, P. *et al.* The Paleoclimate Modeling Intercomparison Project contribution to CMIP5. *CLIVAR Exchanges* **56 (16-2),** 15–19 (2011).
31. Beck, J. *et al.* Sea-surface temperature from coral skeletal strontium/calcium ratios. *Science* **257,** 644–647 (1992).
32. Betts, A. & Miller, M. A new convective adjustment scheme. Part II: Single column tests using GATE wave, BOMEX, ATEX and Arctic air-mass data sets. *Quarterly Journal of the Royal Meteorological Society* **112,** 693–709 (1986).
33. Sahany, S., Neelin, J., Hales, K. & Neale, R. Temperature-moisture dependence of the deep convective transition as a constraint on entrainment in climate models. *Journal of the Atmospheric Sciences* **69,** 1340–1358 (2012).
34. Holloway, C. & Neelin, J. Moisture Vertical Structure, Column Water Vapor, and Tropical Deep Convection. *Journal of the Atmospheric Sciences* **66,** 1665–1683 (2009).
35. Betts, A. & Ridgway, W. Tropical boundary layer equilibrium in the last ice age. *Journal of Geophysical Research* **97,** 2529–2534 (1992).
36. Bryan, G. & Fritsch, J. A Reevaluation of Ice–Liquid Water Potential Temperature. *Monthly Weather Review* **132,** 2421–2431 (2004).
37. Eagle, R. *et al.* High regional climate sensitivity over continental China constrained by glacial-recent changes in temperature and the hydrological cycle. *Proceedings of the National Academy of Sciences* **110,** 8813–8818 (2013).